Applied Physics A (2021) 127:407
https://doi.org/10.1007/s00339-021-04578-7

**Applied Physics A**
**Materials Science & Processing**


# Study of the electrical properties of < 100 > Cz p-type solar-grade silicon wafers against the high-temperature processes

**Mohamed Maoudj[1,2] · Djoudi Bouhafs[1] · Nacer Eddine Bourouba[2] · Abdelhak Hamida-Ferhat[2] · Abdelkader El Amrani[1]**

Received: 30 December 2020 / Accepted: 2 May 2021 / Published online: 11 May 2021


**Abstract**
The aim of this work is to investigate the bulk stability of the solar-grade silicon versus the temperature processing, as well as the surface passivation versus the chemical oxidation. To this end, the quasi-steady-state photo-conductance (QSSPC) measurements showed degradation in minority carrier lifetime ($\tau_{eff}$) after high-temperature processing that involves instability of the silicon wafers face to the thermal processes. Thereby, the bulk investigations indicated the formation of iron–boron (FeB) pairs. These latter are known to be active recombination centers. The FeB pairs formation was highlighted by a study based on sample illumination technique and the crossover point ($\Delta n_{cop}$) identification in the injection-dependent lifetime curves. The surface passivation using both chemical and thermal oxide was used aiming to study the surface properties, in the presence of a thin layer of $SiO_2$. The investigations using the hot probe technique revealed the appearance of an inversion layer, leading to type switching of the semiconductor at the surface, going from p- to n-type. This n-layer induces a high surface recombination velocity (SRV), leading to poor surface passivation. This is caused by the diffusion of the phosphorus toward the silicon surface, induced by the presence of a thin layer of $SiO_2$ in the p-type solar-grade wafers.

**Keywords** FeB pairs · Inversion layer · Oxidation · SRV · $SiO_2$

## 1 Introduction

In the last few years, many alternatives of feedstock production have been developed in the field of microelectronic in general and solar-grade (SoG) silicon in particular, in order to decrease materials costs and energy consumption [1–3]. The features of this SoG-Si are the presence of both dopant elements, viz. the boron and the phosphorus, in the feedstock, which will greatly influence the device properties [3].

Therefore, the low-cost SoG-Si used in industry, commonly known as compensated silicon, contains dopant species and metal impurities, in most cases phosphorous (P), boron (B), and iron (Fe) [4–6]. In 2008, J. Libal et al. [7, 8] argued that solar cell performances that issue from compensated silicon wafers are influenced by the presence of boron and oxygen (B–O) pairs, which are responsible for the phenomenon called light-induced degradation (LID), widely observed in Czochralski silicon wafers [9, 10].

In 2009, F. Rougieux et al. [11] studied the appearance of an inversion layer at the interface $SiO_2$/Si, after thermal oxidation of p-type silicon wafer, and they related this effect to the dopants segregation. The appearance of the n-layer at the interface $SiO_2$/Si has detrimental effects on the device performance. Furthermore, some works affirmed even that the surface recombination has a great negative impact on electrical charge carriers in compensated silicon wafers [12].

This contribution presents an overview of the main solar-grade silicon defects upon a high-temperature processing. For this purpose, different methods have been proposed to study the effect of the thermal processing on iron contamination using the sample illumination technique as well as bulk lifetime ($\tau_b$) calculation, through the computation and simulation of Shockley–Read–Hall (SRH) statistics. The quality of the surface passivation using a thin layer of chemical oxide after post-oxidation annealing (POA) has

✉ Mohamed Maoudj
maomo72@yahoo.fr

[1] CRTSE, Research Centre in Semiconductor Technology for Energetic, 02 Bd Frantz Fanon. BP 140 Alger 7 Merveilles, Algiers, Algeria

[2] Laboratory of Scientific Instrumentation (LIS), Department of Electronics, Faculty of Technology, University Ferhat Abbas, Sétif 1, Sétif, Algeria

been assessed too by the surface recombination velocity simulation.

## 2 Experimental

Boron-doped < 100 > Cz-silicon, 320 µm thick with a resistivity of 1–5 Ω.cm and an initial $\tau_{eff}$ of 13.5 µs, was used. The surface wafers were cleaned using the conventional chemical cleaning followed by the piranha etch treatment prior to $SiO_2$ processing. The batch of the wafers was divided into two groups. The first one was subjected to thermal oxidation at 850 °C, 900 °C, 950 °C, and 1000 °C with an oxide thickness of 10 nm in a quartz tube furnace using $N_2/O_2$ gas flow. The second group was thermally annealed for 30 min in high-purity nitrogen ($N_2$) atmosphere.

Afterward, the QSSPC measurements were used to assess the minority carrier lifetime ($\tau_{eff}$) of the different processed wafers.

The iron contamination of the wafers was highlighted by the dissociation of FeB pairs formed from interstitial iron ($Fe_i$) under the annealing effect at 1000 °C.

This method outlined by MacDonald et al. [13] is based on the crossover of the injection-dependent lifetime curves, measured before and after iron–boron pair dissociation under illumination.

On the other hand, the surface passivation was analyzed by SRV simulation; in this study, a decoupling method of bulk lifetime and SRV was used in order to impact assessment of the presence of a thin oxide layer on the surface of silicon wafers.

In order to study the influence of the silicon oxidation on the quality of the surface passivation, we adopted a comparative study using chemical oxidation following the nitric acid oxidation of silicon (NAOS) process [14] and the iodine–ethanol (I–E) solution at a molar concentration of 0.02 mol/L [15, 16]. These two methods allow suitable surface passivation and stability of the parameters related to the bulk.

## 3 Results and discussion

### 3.1 Influence of the thermal oxidation on minority carrier lifetime

The influence of the high-temperature oxidation on the minority carrier lifetime has been highlighted, by growing 10-nm thin film of thermal $SiO_2$ at different temperatures: 850 °C, 900 °C, 950 °C, and 1000 °C. The QSSPC results,

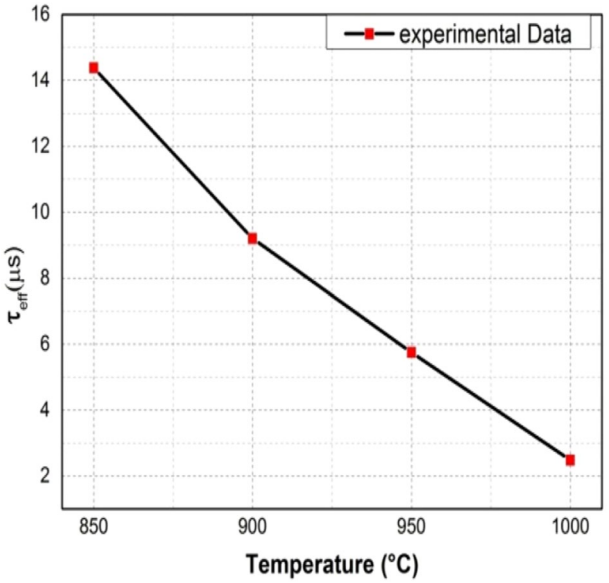


**Fig. 1** $\tau_{eff}$ degradation at different oxidation temperatures (850–1000 °C) on < 100 > p-type silicon wafer

showing the influence of the oxidation temperature on the minority carrier lifetime, are presented in Fig. 1.

As it can be seen, the minority carrier lifetime decreases drastically with oxidation temperature and reaches a $\tau_{eff}$ equal to 2.48 µs at the temperature processing of 1000 °C, at the injection level of $1 \times 10^{15}$ $cm^{-3}$.

The effective lifetime ($\tau_{eff}$) includes both surface and bulk components. It is described according to the following equation:

$$1/\tau_{eff} = 1/\tau_{bulk} + (2S_{eff})/W \quad (1)$$

where $S_{eff}$ is the surface recombination velocity and W is the wafer thickness. Therefore, recombinations occur in the bulk as well as on both surfaces of the silicon wafers.

The hot-probe analysis after thermal oxidation reveals the apparition of an inversion layer at the wafer surfaces, leading to a switch of semiconductor type from p- to n-type. The hot-probe method is performed by contacting a semiconductor wafer with a hot and a "cold" probe. This will generate a thermal gradient, which will give rise to an electric current in the semiconductor.

Depending on the semiconductor type, the current read from a galvanometer will be negative or positive [11]. This technique is very useful to quickly check the presence of an inversion layer at the surface of the wafer.

In the following section, we will highlight how the temperature influences the bulk lifetime as well as the surface passivation in p-type solar-grade silicon.

## 4 Analysis of iron contamination

In order to study the influence of the iron impurities on effective lifetime, the wafers were annealed at 1000 °C in high-purity nitrogen ($N_2$) atmosphere. Thereafter, the wafers were immersed in a 5wt% HF solution for 10 s to avoid any oxide formation.

The thermal processing at 1000 °C under $N_2$ ambiance resulted in a degradation of minority carrier lifetime until 4.51 µs. It should be noted that the annealing exceeding the temperature of 1000° C did not record any variation in $\tau_{eff}$.

However, the illumination of the annealed samples allowed an increase in $\tau_{eff}$ from 4.51 to 14.5 µs, as shown in Fig. 2.

It should be pointed out that the wafers prepared in this section will be used as a reference, in the part devoted to the surface passivation study.

The detection of metallic contamination has been highlighted by the illumination of the annealed samples using the flash of the QSSPC instrument with an intensity of 25 W/cm$^2$ at room temperature. The illumination methods are well established and based on the photodissociation of iron–boron (FeB) pairs, which are formed from interstitial iron ($Fe_i$). The dissociation behavior was observed around a crossover point as depicted in Fig. 3.

The formation and dissociation of FeB pairs are described by the following equations:

$$Fe_i^+ + B^- \rightarrow FeB \quad (2)$$

$$FeB + e^- \rightarrow Fe_i^0 + B^-. \quad (3)$$

More details can be found elsewhere [17, 18].

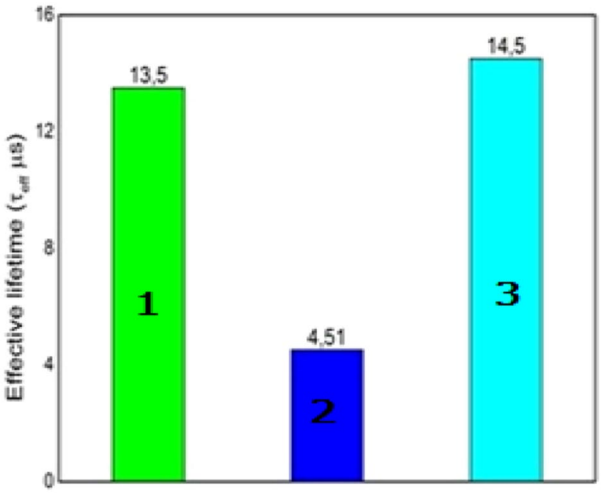


**Fig. 2** Evolution of the effective minority carrier lifetime ($\tau_{eff}$) during the adopted protocol. 1 represents initial value, 2—after annealing, and 3—after illumination

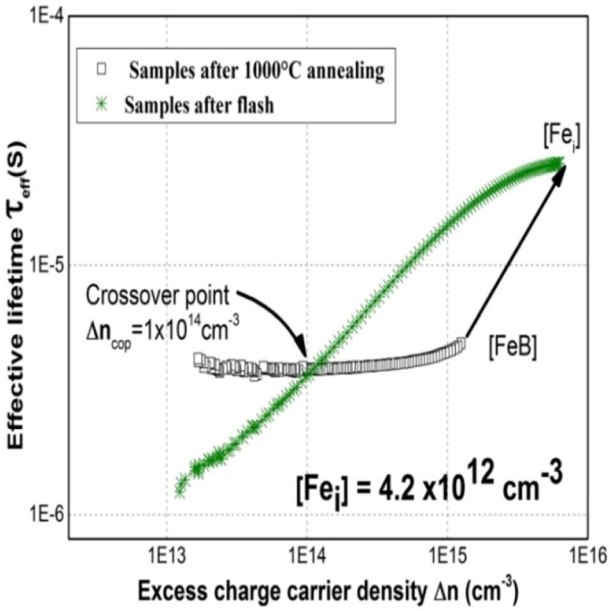


**Fig. 3** $\tau_{eff}$ enhancement after illumination assessed by means of the QSSPC instrument on p-type silicon wafer annealed at 1000 °C

Under the assumption that the complete formation of FeB pairs (100% FeB pairs) is dissociated after illumination (100% $Fe_i$). Figure 3 depicts the influence of illumination on the minority carriers lifetime involving the phenomenon of the $Fe_i$ dissociation and the FeB association. So, the (FeB) pairs dissociation results in an increase in minority lifetime at high injection levels and a decrease at low injection levels. Thence, the curves exhibit a crossover point near $1.1\times10^{14}$ cm$^{-3}$.

The mechanisms of FeB association and dissociation can be explained by the fact that, under the illumination effect, the FeB pairs dissociate and give rise to a maximum of interstitial iron concentration [$Fe_i$].

When calculated according to Eq. 4, a value of $4.2\times10^{12}$ cm$^{-3}$ was found for this latter, hence increasing the minority carrier lifetime. The $\tau_{eff}$ enhancement is associated with the fact that the FeB pairs theory does not allow an association of iron–boron under illumination, because the quasi-Fermi level exceeds the interstitial iron energy-level position [3]. In other words, the interstitial iron is neutrally charged during illumination and no Coulombic attraction occurs between iron and boron [13, 17, 18]. So, this will have a consequence on $\tau_{eff}$ enhancement.

Note that the calculation of $Fe_i$ concentration is provided by Eq. (4) following the Zoth and Bergholz works [13].

$$[Fe] = A\left(\frac{1}{L_1^2} - \frac{1}{L_0^2}\right) = C\left(\frac{1}{\tau_1} - \frac{1}{\tau_0}\right). \quad (4)$$

The prefactor A is determined empirically to be $1.06\times10^{16}$ µm$^2$ cm$^{-3}$ for silicon wafers of resistivity range

from 5 to 15 Ωcm. If the low-injection carrier lifetime (τ) is measured rather than the diffusion length, case of this study, then the prefactor C is related to A via $A = D_n C$, where $D_n$ is the minority carrier diffusion coefficient. $\tau_0$ and $\tau_1$ represent, respectively, the minority carrier lifetime before and after illumination [13].

According to the study of MacDonald et al. [13], the position of the crossover point at $1 \times 10^{14}$ cm$^{-3}$ can be used as an unambiguous fingerprint for the detection of the iron contamination in p-type silicon wafer when the boron concentration is below $5 \times 10^{16}$ cm$^{-3}$ [13, 19, 20].

As the FeB pairs are considered as the main bulk recombination centers, the modeling of the injection-dependent lifetime $\tau_{FeB} = f(\Delta n)$ following the Shockley–Read–Hall (SRH) statistics is given by equation:

$$\frac{1}{\tau_{SRH}} = \frac{(N_A + \Delta n)}{\tau_{p0}(n_1 + \Delta n) + \tau_{n0}(N_A + p_1 + \Delta n)}. \quad (5)$$

Here, $N_A \simeq 9 \times 10^{15}$ cm$^{-3}$, $\Delta n = \Delta p$ is the excess carrier density, and $\tau_{n0}$ and $\tau_{p0}$ are the fundamental electron and hole lifetimes, which are related to the following parameters: recombination center density, the thermal velocity [21, 22]: $v_{th} = 1 \times 10^7$ cm/s, and the capture cross sections via $\tau_{n0} = 1/(v_{th}\, \sigma_n\, N_{SRH})$ and $\tau_{p0} = 1/(v_{th}\, \sigma_p\, N_{SRH})$.

When the Fermi energy level coincides with the defect energy level, the electron and hole densities, $n_1$ and $p_1$, are defined by:

$$n_1 = Nc \exp\left(\frac{E_T - E_c}{KT}\right) \quad (6)$$

$$p_1 = Nv \exp\left(\frac{E_c - E_G - E_T}{KT}\right). \quad (7)$$

Values for the effective densities of states at the conduction and valence band edges are taken as $N_C = 2.86 \times 10^{19}$ cm$^{-3}$ and $N_V = 3.1 \times 10^{19}$ cm$^{-3}$ [21, 23].

The recombination parameters used for modeling the injection-dependent lifetime $\tau_{FeB} = f(\Delta n)$ are given in Table 1.

The injection-dependent lifetime related to the FeB recombination centers is represented in Fig. 4, from which one can easily determine $\tau_b = \tau_{SRH} = \tau_{FeB}$ at different injection levels. We can therefore deduce $\tau_b = 5.9$ µs at $\Delta n = 1 \times 10^{15}$ cm$^{-3}$; this latter will be very useful for the rest of this work.

**Table 1** Energy levels and capture cross sections for $Fe_i$ and the acceptor states of FeB pairs based on MacDonald et al.'s studies [22]

| Recombination centers | Energy level (ev) | $\sigma_n$ (cm$^{-2}$) | $\sigma_p$ (cm$^{-2}$) |
|---|---|---|---|
| $Fe_i$ | $E_V + 0{,}38$ | $5 \times 10^{-14}$ | $7 \times 10^{-17}$ |
| FeB acceptor | $E_C - 0{,}23$ | $3 \times 10^{-14}$ | $2 \times 10^{-15}$ |

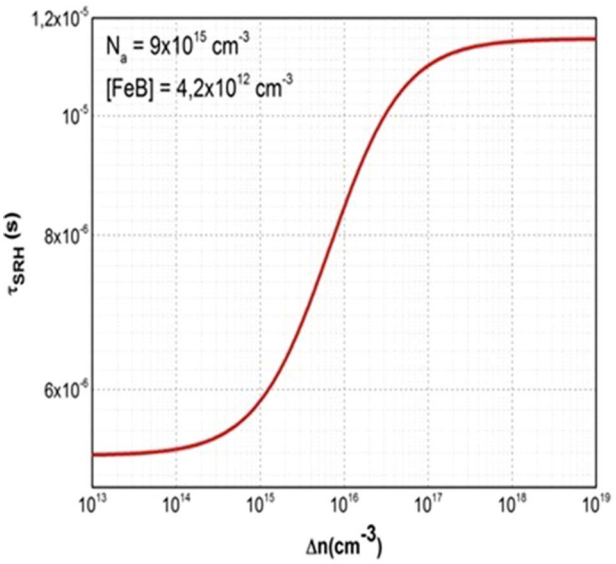


**Fig. 4** Simulation of SRH injection-level-dependent lifetime curve for FeB pairs in p-type silicon wafer, with a resistivity of 1–3 Ω cm. The density of FeB centers has been taken equal to $4.2 \times 10^{12}$ cm$^{-3}$

## 5 Investigation of surface passivation using chemical $SiO_2$ thin layer

The previous study allowed to state that the temperature processing alters the bulk of the silicon wafers due primarily to the formation of FeB pairs, which represent the predominant recombination centers.

In the present section, the wafers used in the previous study (Sect. 2) have been taken up, but after spent a 24-h relaxation in the dark for a total recovery. Hereafter, in order to avoid any change in the electrical parameters of the bulk, a surface passivation using chemical oxidation was carried out according to the nitric acid oxidation (NAOS) process. Then, the wafers sustained a post-oxidation annealing (POA) at 850 °C under high-purity $N_2$ gas in order to activate the surface passivation.

However, for a good assessment of the surface passivation, we have undertaken a comparison between two ways of surface passivation. So, additionally to the chemical oxidation, the surface passivation using iodine–ethanol (I–E) solution was carried out.

The first step of the protocol consisted of applying passivation using I–E, and after wafers cleaning, a chemical oxidation was carried out on these same samples.

It should be mentioned that after the chemical oxidation followed by the POA process, hot-probe analysis revealed

the apparition of an inversion layer on the surface of the wafers. Therefore, the following study is an investigation of the influence of this n-layer on the surface passivation.

The quality of the surface passivation has been assessed by SRV simulation, according to the following expression [24, 25]:

$$\frac{1}{\tau_{eff}} = \frac{1}{\tau_{bulk}} + \left[\frac{W}{2S} + \frac{1}{D_n}\left(\frac{W}{\pi}\right)^2\right]^{-1}. \quad (8)$$

Figure 5 shows the variation of $\tau_{eff}$ as a function of the SRV for a determined bulk lifetime. $\tau_b$ is taken equal to 5.9 µs at $\Delta n = 1 \times 10^{15}$ cm$^{-3}$.

($\tau_b$ is deduced from Fig. 4).

On the other hand, Fig. 6 shows the injection-dependent lifetime curves for the two surface passivation schemes, namely the chemical oxidation and iodine–ethanol solution. The main results from the different measurements and simulation are summarized in Table 2.

The adopted method for SRV determination is a straightforward reading of $\tau_{eff}$ at $\Delta n = 1 \times 10^{15}$ cm$^{-3}$ from Fig. 6 and then match it the adequate SRV from Fig. 5.

The results presented in Table 2 indicate that the surfaces passivated using iodine–ethanol gave a relatively better passivation quality than the surfaces passivated using chemical oxidation. This latter with a thin chemical $SiO_2$ layer of 2 nm resulted in a $\tau_{eff}$ of about 1 µs and a strong SRV compared to

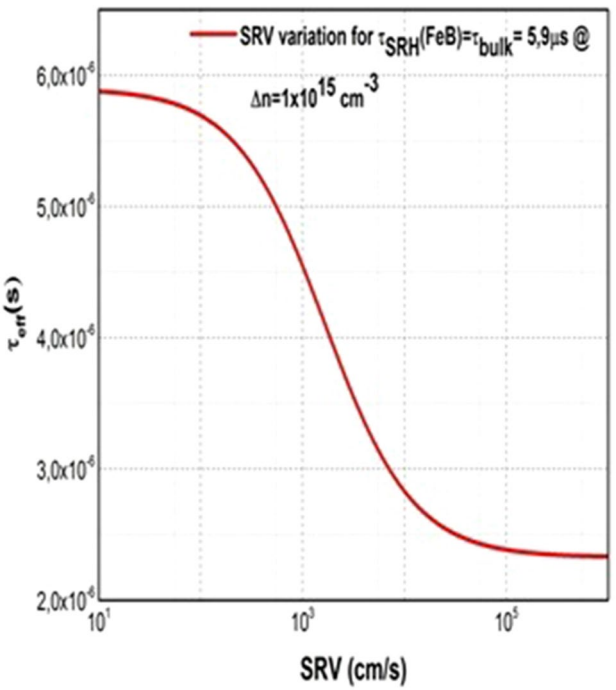


**Fig. 5** Simulation of effective minority lifetime vs surface recombination velocity at $\Delta n = 1 \times 10^{15}$ cm$^{-3}$ with $\tau_b = 5.9$ µs

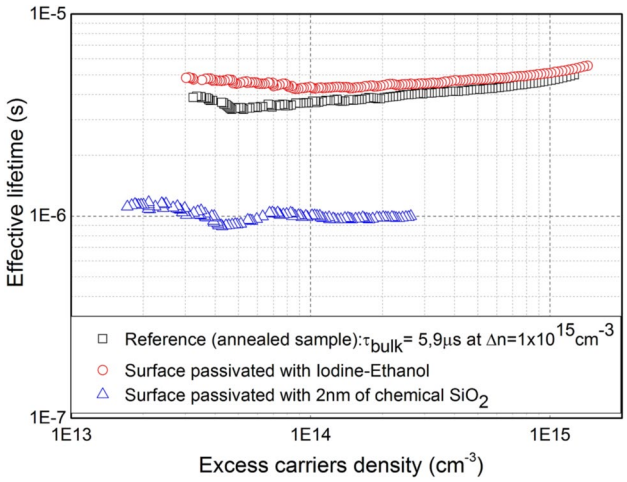


**Fig. 6** Injection-dependent lifetime curves at different schemes passivation with $\tau_{bulk} = 5.9$ µs. Recall that the samples have been annealed at 1000 °C

the I–E results, which gave a $\tau_{eff}$ of 5.12 µs with a decrease in SRV from 874 cm/s (reference sample) to 450 cm/s. The excess minority carrier for the oxidized wafers is also too weak ($\Delta n_{max} = 1 \times 10^{14}$ cm$^{-3}$), which indicates poor surface passivation.

These results are evidence that degradation in the quality of surface passivation occurred in wafers passivated by a thin layer of chemical $SiO_2$, compared to the surface passivated by the I–E solution, given that $\tau_{bulk}$ remained invariant.

It is worth pointing that the difference between these two types of passivation is the appearance of the oxide-induced inversion layer in the oxidized samples. Therefore, it is the obvious reason for the degradation of the surface passivation using $SiO_2$.

The inversion layer is attributed to an accumulation of phosphorus at the surface of compensated silicon. The reason is the equilibrium segregation coefficient of the boron ($m_{boron}$) at the $SiO_2$/Si interface, which is equal to approximately 0.3, meaning that the oxide attracts boron. As $m_{phosphorus} = 10$, this implies that the oxide repels phosphorus [26].

Based on these results, one can state that during the oxide growth, boron tends to become depleted at a specific depth

**Table 2** Surface parameters deduced from effective minority lifetime versus surface recombination velocity (SRV) (Fig. 5) and the injection-dependent lifetime curves (Fig. 6), according to the two ways of the surface passivation.

| Process method | $\tau_{eff}$ (µs) | SRV (cm/s) |
|---|---|---|
| Reference (annealed sample) | 4.51 | 874 |
| I–E passivation | 5.12 | 450 |
| $SiO_2$ passivation | 1 | SRV > > > |

from the surface, while phosphorus tends to pile up just below the surface. In non-compensated p-type silicon, this phenomenon induces a depletion zone free of boron near the interface. But in compensated p-type silicon, it leads to phosphorous accumulation [11]. As phosphorus is a donor impurity, it seems that it will give an additional interface state density ($D_{it}$) responsible for the degradation of the surface passivation using $SiO_2$.

## 6 Conclusion

In this paper, it was shown that compensated silicon, although it is a good alternative in terms of cost, cannot be effective in terms of quality.

The investigations carried out in this work have shown that the minority carrier lifetime ($\tau_{eff}$) is strongly influenced by the temperature processing, which is an unavoidable factor in all technological processes as well as the appearance of an inversion layer induced by oxidation.

Thus, the degradation of $\tau_{bulk}$ is dominated by the presence of the interstitial iron impurity, which under the temperature effect gives rise to (FeB) pairs; these are known to be very active recombination centers introducing trap levels in the band gap according to the SRH statistics. On the other hand, a simple and effective method has been proposed in this work, allowing the decoupling of $\tau_{bulk}$ and SRV based on the modeling of experimental data, in order to study the influence of the inversion layer induced by the oxidation on the SRV.

For this purpose, two passivation routes have been implemented in a comparative way. The results showed an enhancement in minority carrier lifetime with a diminution of surface recombination velocity in the samples passivated with I–E solution. In contrast, the oxidation of the same samples using chemical oxidation according to the NAOS protocol followed by POA revealed poor surface passivation. The high value of the surface recombination velocity and a significantly low value of $\tau_{eff}$ reveal a bad surface passivation compared to those obtained with I–E solution. The degradation of the surface passivation can be attributed to the appearance of an n-layer at the silicon surface, caused by doping segregation during the oxide growth and giving rise to an additional interface state density ($D_{it}$).

**Acknowledgements** The authors gratefully acknowledge the financial support from the Directorate General for Scientific Research and Technological Development (DGRSDT–Algerian Ministry of Higher Education and Scientific Research).

## References

1. V. Hoffmann, K. Petter, J. Djordjevic-Reiss, E. Enebakk, J.D. Håkedal, R. Tronstad, T. Vlasenko, I. Buchovskaja, S. Beringov, M. Bauer, 23rd EUPVSEC, Valencia. Spain (2008). https://doi.org/10.4229/23rdEUPVSEC2008-2BO.3.3
2. D. Sarti, R. Einhaus, Sol. Ener. Mater. Sol. Cells. (2002). https://doi.org/10.1016/S0927-0248(01)00147-7
3. S. Rein, J. Geilker, W. Kwapil, G. Emanuel, I. Reis, A.K. Soiland, S. Grandum, R. Tronstad, 25th EUPVSEC and Exhibition, Valencia. Spain (2010). https://doi.org/10.4229/25thEUPVSEC2010-2BO.1.2
4. T. Bartel, K. Lauer, M. Heuer, M. Kaes, M. Walerysiak, F. Gibaja, J. Lich, J. Bauerd, F. Kirscht, Energy Procedia **27**, 45–52 (2012)
5. S. Pizzini, Sol. Ener. Mater. Sol. Cells (2010). https://doi.org/10.1016/j.solmat.2010.01.016
6. D. MacDonald, A. Liu, A. Cuevas, B. Lim, J. Schmidt, Phys Status Solidi A: Appl. Mater. Sci. (2011). https://doi.org/10.1002/pssa.201000146
7. S. Rein, W. Kwapil, J. Geilker, G. Emanuel, M. Spitz, I. Reis, A. Weil, D. Biro, A.K. Soiland, E. Enebakk, R. Tronstad, 24th EUPVSEC, Hamburg. Germany (2009). https://doi.org/10.4229/24thEUPVSEC2009-2DO.2.3
8. J. Libal, S. Novaglia, M. Acciarri, S. Binetti, R. Petres, J. Arumughan, R. Kopecek, A. Prokopenko, J. App. Phys. (2008). https://doi.org/10.1063/1.3021300
9. S. Rein, S.W. Glunz, Appl. Phys. Lett. **82**(7), 1054–1056 (2003)
10. K. Bothe, J. Schmidt, R. Hezel, 3rd WCPEC, Osaka. Japan (2003). https://doi.org/10.1109/WCPEC.2003.1306099
11. F. Rougieux, D. Macdonald, K.R. Mcintosh, A. Cuevas, 24th EUPVSEC, Hamburg. Germany (2009). https://doi.org/10.4229/24thEUPVSEC2009-2CO.3.6
12. A. Cuevas, IEEE Conference on Optoelectronic and Microelectronic Materials and Devices (2002). https://doi.org/10.1109/COMMAD.2008.4802135
13. D. Macdonald, L. Geerligs, A. Azzizi, J. Appl. Phys. (2004). https://doi.org/10.1063/1.1637136
14. H.A. Kobayashi suha, O. Maida, M. Takahashi, H. Iwasa, J. Appl. Phys. (2003). https://doi.org/10.1063/1.1621720
15. N. Khelifati, D. Bouhafs, A. Mebarek-Azzem, S.E.-H. Abaidia, B. Palahouane, Y. Kouhlane, Acta Phys. Pol A (2016). https://doi.org/10.12693/APhysPolA.130.188
16. J. W. Chen, L. Zhao, H. Diao, B. Yan, S. Zhou, Y. Tang and W. Wang, Adv. Mat. Res. (2013). https://doi.org/10.4028/www.scientific.net/AMR.652-654.901
17. M. Maoudj, D. Bouhafs, N. Bourouba, N. Khelifati, A. El Amrani, R. Boufnik, A. Hamida-Ferhat, Acta Phys. Pol A (2017). https://doi.org/10.12693/APhysPolA.132.725
18. X. Zhu, X. Yu, P. Chen, Y. Liu, J. Vanhellemont, D. Yang, Int. j. photoenergy. (2015). https://doi.org/10.1155/2015/154574
19. D. Macdonald, T. Roth, P.N.K. Deenapanray, Appl. Phys. Lett. **89**, 142107 (2006)
20. C. Möller, A. Laades, K. Lauer, Solid State Phenom. **205**, 265 (2014)
21. D. Macdonald, A. Cuevas, J. Wong-Leung, J. App. Phys. **89**, 12 (2001)
22. W.M. Bullis, H.R. Huff, J. Electrochem. Soc. **143**, 1399 (1996)
23. M.A. Green, J. Appl. Phys. **67**, 2944 (1990)
24. S. Rein, Lifetime spectroscopy, A Method of Defect Characterization in Silicon for Photovoltaic Applications 1st edn. (Springer 2005), pp. 50–53.
25. A.B. Sproul, J. Appl Phys. (1994). https://doi.org/10.1063/1.357521
26. A.S. Grove, O. Leistiko, C.T. Sah, J. Appl. Phys. (1964). https://doi.org/10.1063/1.1713825